Journal of Alloys and Compounds 705 (2017) 98–104

Contents lists available at ScienceDirect

Journal of Alloys and Compounds

journal homepage: http://www.elsevier.com/locate/jalcom

Martensitic transformation behaviors and mechanical properties of $(Ti_{36}Ni_{49}Hf_{15})_{100-x}Y_x$ high temperature shape memory alloys

Xiaoyang Yi, Weihong Gao, Xianglong Meng*, Zhiyong Gao, Wei Cai, Liancheng Zhao

School of Materials Science and Engineering, Harbin Institute of Technology, Harbin, 150001, China

ARTICLE INFO

Article history:
Received 22 December 2016
Received in revised form
8 February 2017
Accepted 12 February 2017
Available online 16 February 2017

Keywords:
Ti-Ni-Hf alloy
High temperature shape memory alloy
Martensitic transformation
Shape memory effect
Microstructure

ABSTRACT

Martensitic transformation and shape memory effect (SME) of the $(Ti_{36}Ni_{49}Hf_{15})_{100-x}Y_x$ alloys are investigated. It is found that all the samples undergo martensitic transformation from cubic parent phase (B2) to monoclinic martensite (B19′). The Y addition slightly decreases the phase transformation temperatures mainly due to the low solid solubility limit of Y in Ti-Ni-Hf alloys. The micro-hardness and compressive strength are enhanced as a result of the Y addition. The SME increases firstly with increasing Y content up to 2.0 at.% and then decreases with the further increased Y content. The obtained maximum completely recoverable strain is 4% obtained for Y content higher than 1 at.%.

1. Introduction

Recently, extensive researches regarding the high temperature shape memory alloys (HTSMAs) have been carried out in order to meet the increased demands for the high temperature applications such as robotic, automotive and aerospace industries [1,2]. The Ti-Ni-Hf HTSMAs are highly desirable for the high temperature engineering applications owing to their high martensitic transformation temperatures, high work outputs and relative lower cost [2–5]. Usually, the Hf content of Ti-Ni-Hf alloys is more than 10 at.% to get a sufficient martensitic transformation start (M_s) temperature [6]. However, in that case, the SME of Ti-Ni-Hf based alloys is poor (~3%) due to the low matrix strength [7]. Such a poor SME is far lower than that of the commercial Ti-Ni binary alloy, which hinders their broad applications to some extent. Thermo-mechanical treatment, precipitation hardening and adding the quaternary element are the main methods to enhance the strength of matrix for Ti-Ni based alloys [5,8,9]. Due to the brittle feature of Ti-Ni-Hf alloy, it is very hard to conduct cold-work [7]. As reported, the shape memory properties can be improved in slightly Ni-rich Ti-Ni-Hf alloys through precipitation of fine particles by aging [7,10–12]. The maximum recoverable strain of about 3% can be obtained in both the aged Ni-rich Ti-Ni-Hf polycrystalline alloy and the aged [111]-orientation Ni-rich Ti-Ni-Hf single crystalline alloy [7,13]. Several quaternary alloying elements including Cu, Pd and Nb etc. have been added into the Ti-Ni-Hf alloys [14–18]. The addition of these elements decreases the martensitic transformation temperatures of Ti-Ni-Hf alloys and slightly improves the SME with a maximum value of around 3% [14–16]. It is well known that both the grain refinement and solution strengthening could enhance the strength of alloys. At the same time, it has been confirmed that adding rare earth element into Ti-Ni shape memory alloys not only increases the transformation temperatures [19], but also improves the shape memory effect [20]. Hence, it is highly expected to improve the mechanical properties and simultaneously increase the transformation temperatures, or at least without dramatically decreasing the transformation temperatures by means of adding the quaternary element Y to Ti-Ni-Hf alloy.

In the present study, the effect of Y addition on the phase transformation behaviors, microstructure and mechanical properties in the Ti-Ni-Hf based alloys have been systematically investigated.

2. Experimental procedure

$(Ti_{36}Ni_{49}Hf_{15})_{100-x}Y_x$ (x = 0, 0.5, 1.0, 2.0, 2.5 at.%) ingots (~50 g) were prepared by vacuum arc melting furnace. To ensure chemical composition homogeneous, the ingots were remelted five times,

* Corresponding author.
E-mail address: xlmeng@hit.edu.cn (X. Meng).

http://dx.doi.org/10.1016/j.jallcom.2017.02.137
0925-8388/

and then homogenized at 1173 K for 3 h in vacuum, followed by rapid quenching in water. Phase transformation behaviors were detected by differential scanning calorimetry (DSC) with a heating and cooling rate of 20 K/min between 323 K and 573 K. Phase identification was examined using X-ray diffraction (XRD) method with Cu K_α radiation at room temperature. Microstructures were characterized by scanning electron microscope (SEM) equipped with energy dispersive spectroscopy (EDS). The SEM images were taken under backscattered electron (BSE) mode. The samples for SEM observations were etched by a solution of HF: HNO_3: H_2O = 1: 4: 5 (vol). TEM observations were executed using a Philips FEI Tecnai G^2F20S-TWIN electron microscope equipped with a double-tilt platform at 300 kV. The thin-foil specimens for TEM observations were prepared by twin-jet electro-polished with the solution of 20% H_2SO_4 by volume in CH_3OH at around 253 K.

Hardness was characterized by the Vickers micro-hardness with test parameter: 200 g loading and holding for 20 s at room temperature. The values of hardness are the average of at least 15 measures for each sample. The shape memory effect was characterized by compression test. The specimens of compression were small cylinders with a gage size φ 3 mm × 5 mm. The original samples (L_0 = 5 mm) were compressed to L_1 at a rate of 0.2 mm/min, which was conducted in Instron-5569. The height of sample after unloading was supposed as L_2. And then lasted for 5 min at 550 K in heating furnace. The height of specimen was defined as L_3 at the moment. The measurement procedure was shown schematically in Figure 1(a). Fig. 1(b) represented the typical compressive stress-strain curve during loading and unloading for 8% deformation in Ti-Ni-Hf-Y alloys. The elastic strain (ε_{el}) was measured by the following equation: $\varepsilon_{el} = (L_2\text{-}L_1)/L_0 \times 100\%$. While, the shape memory effect (ε_{sme}) was characterized by the following formula: $\varepsilon_{re} = (L_3\text{-}L_2)/L_0 \times 100\%$, the recoverable strain (ε_{re}) was characterized by the formula: $\varepsilon_{re} = \varepsilon_{sme} + \varepsilon_{re}$.

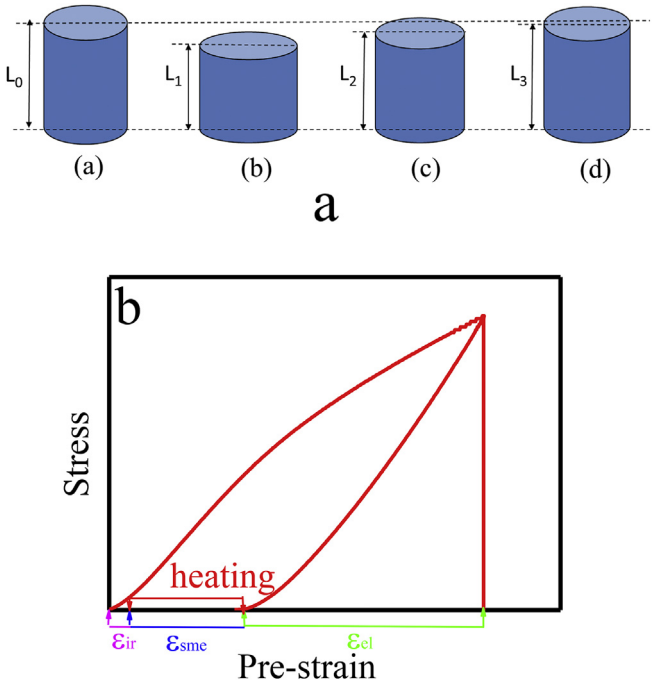

Fig. 1. a: Schematic illustration of shape memory effect measurement. (a): Original sample's height, L_0. (b): Sample's height after applying certain compressive strain, L_1. (c): Sample's height after unloading, L_2. (d): Sample's height after holding at 550 K for 5 min, L_3. b: The typical stress-strain curve during loading and unloading for 8% deformation in the solution-treated $(Ti_{36}Ni_{49}Hf_{15})_{100\text{-}x}\text{-}Y_x$ alloys.

3. Results and discussion

3.1. Microstructural analysis

Fig. 2 shows the XRD patterns of the solution-treated $(Ti_{36}Ni_{49}Hf_{15})_{100\text{-}x}\text{-}Y_x$ alloys at ambient temperature. It can be seen that all the samples are the monoclinic martensite phase (B19′) without any obviously observed second phase within the detection limit of XRD spectrometer, which indicates that the M_s temperatures are above room temperature. The lattice constant of the martensite for all samples almost keeps constant (a = 0.2450 nm; b = 0.4082 nm; c = 0.4778 nm, β = 99.32°). The results obtained from the XRD patterns suggest that Y addition does not obviously change the crystal structure and lattice constant for the solution-treated $(Ti_{36}Ni_{49}Hf_{15})_{100\text{-}x}\text{-}Y_x$ alloys. It can be seen from the Table 1 that the solid solubility limit of Y in the matrix is less than 0.2 at.% for the Ti-Ni-Hf alloy, thus, no obvious variation in crystal structure and lattice constant can be found even though the atomic radius of Ti (0.2 nm), Ni(0.162 nm), Hf (0.216 nm) and Y(0.227 nm) is distinct. Similarly, for binary Ti-Ni alloy, the solid solubility limit of Y in the matrix is lower and the crystal structure with monoclinic martensite (B19′) of Ti-Ni remains unchanged [19].

Fig. 3 shows the backscattered electron micrographs of the solution-treated $(Ti_{36}Ni_{49}Hf_{15})_{100\text{-}x}Y_x$ alloys. All the samples consist of the matrix phase (bright) and the second phase (dark). The second phases primarily distribute along the grain boundaries. The amount of the second phase increases with the increased Y content. The microstructure varies from scattered dendritic distribution to a compact network connection with the Y content increasing. Fig. 3f shows an enlarged image of the second phase with an irregular shape. The chemical compositions of the matrix and second phase of the $(Ti_{36}Ni_{49}Hf_{15})_{100\text{-}x}Y_x$ alloys measured by the EDS analysis are listed in Table 1. The results show that the solid solubility limit of Y in the matrix is lower than 0.2 at.% and Y is mainly rich in the second phase. The lower solid solubility limit of Y in the matrix may be attributed to the large atom size of Y. Besides, it is notable that the grain size strongly depends on the Y content in the present $(Ti_{36}Ni_{49}Hf_{15})_{100\text{-}x}Y_x$ alloys. The grain size decreases approximately from 60 μm to 20 μm when Y content increases from 0 at.% to 2.5 at.%, as shown in Fig. 4. The grain refinement caused by Y addition may improve the mechanical properties of the solution treated $(Ti_{36}Ni_{49}Hf_{15})_{100\text{-}x}Y_x$ alloys.

Fig. 5 shows the typical TEM bright-field (BF) micrographs and the corresponding selected area electron diffraction (SAED) patterns

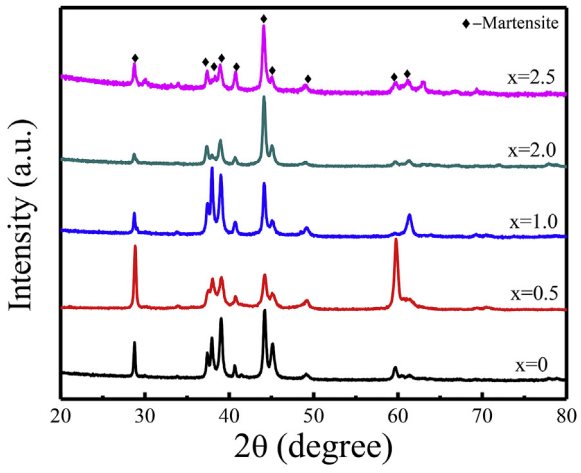

Fig. 2. XRD patterns of the solution-treated $(Ti_{36}Ni_{49}Hf_{15})_{100\text{-}x}\text{-}Y_x$ alloys.